Lab on a Chip

Numerical design and optimization of hydraulic resistance and wall-shear stress inside pressure-driven microfluidic networks

Journal:	*Lab on a Chip*
Manuscript ID:	LC-ART-05-2015-000578.R1
Article Type:	Paper
Date Submitted by the Author:	07-Aug-2015
Complete List of Authors:	Damiri, Hazem; The University of Jordan, Mechanical Engineering Department, Faculty of Engineering and Technology Bardaweel, Hamzeh; Institute for Micromanufacturing, College of Engineering and Science, Louisiana Tech University

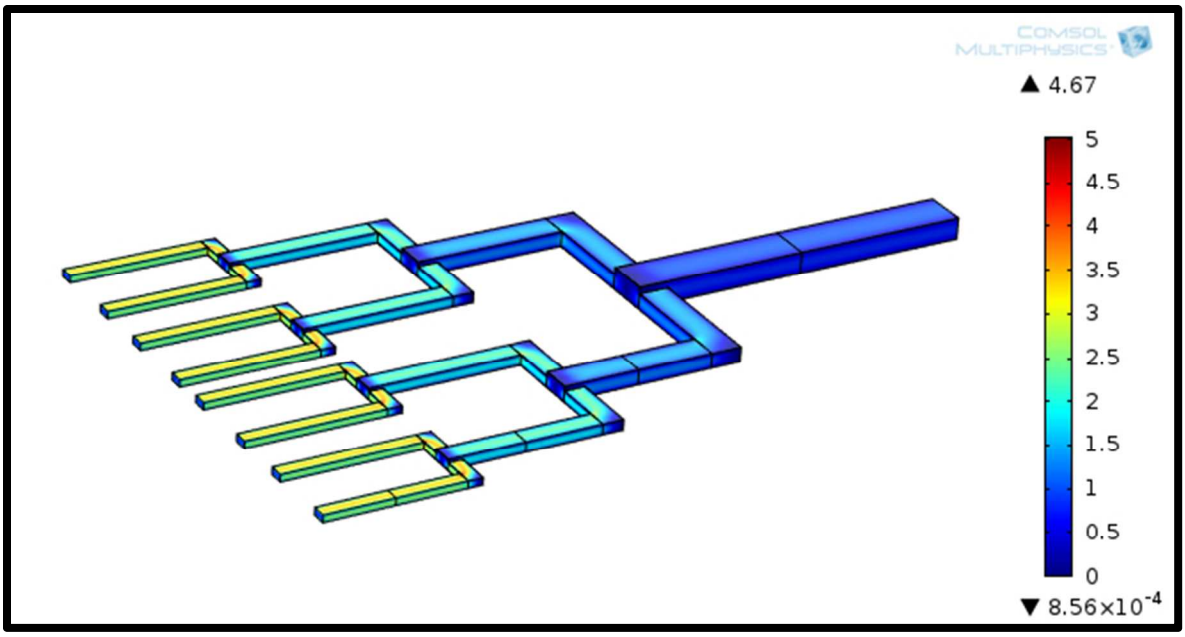

Control of total wall shear-stress in n-generation microfluidic network.

Numerical design and optimization of hydraulic resistance and wall-shear stress inside pressure-driven microfluidic networks

Hazem Damiri[1] & Hamzeh Bardaweel [*, 2]

[1] Department of Mechanical Engineering,

Faculty of Engineering and Technology,

The University of Jordan,

Amman, Jordan.

[2] Institute for Micromanufacturing,

College of Engineering and Science,

Louisiana Tech University,

Ruston, Louisiana 71272

United States.

[*] Corresponding author.

ABSTRACT

Microfluidic networks represent the milestone of microfluidic devices. Recent advancements in microfluidic technologies mandate complex designs where both hydraulic resistance and pressure drop across the microfluidic network are minimized while wall shear-stress is precisely mapped through the network. In this work, a combination of theoretical and modeling techniques is used to construct a microfluidic network that operates under minimum hydraulic resistance and minimum pressure drop while gagging wall shear-stress through the network. The results show that in order to minimize hydraulic resistance and pressure drop throughout the network while constant wall shear-stress through the network is maintained, geometric and shape conditions related to compactness and aspect ratio of parent and daughter branches must be followed. Also, results suggest that while a “local” minimum hydraulic resistance can be achieved for a geometry with arbitrary aspect ratio, a "global" minimum hydraulic resistance occurs, only, when the aspect ratio of that geometry is set to unity. Thus, it is concluded that square and equilateral triangular cross-sectional area microfluidic networks have the least resistances compared to all rectangular and isosceles triangular cross-sectional microfluidic networks, respectively. Precise control over wall shear-stress through the bifurcations of the microfluidic network is demonstrated in this work. Three multi-generation microfluidic network designs are considered. In these three designs wall shear-stress in the microfluidic network is, successfully, kept constant, increased in the daughter-branch direction, or decreased in the daughter-branch direction, respectively. For the multi-generation microfluidic network with constant wall shear-stress, design guidelines presented in this work result in identical profiles of wall-shear stresses not only within a single generation but, also, through all the generations of the microfluidic network under investigation. The results obtained in this work are consistent with previously reported data and suitable for wide range of lap-on-chip applications.

INTRODUCTION

Chief among microfluidic developing technologies is bio-microfluidic devices inspired by biological systems found in living organs in nature [1, 2]. For example, a great effort has been put forward by several groups to mimic organs found in mammals such as kidney [2] and lung [1, 3]. Often, this is referred to as *Organ-on-a-chip*. The so called *organ-on-a-chip* consists of several chambers filled with specified cell cultures and connected through a network of micro-channels [4]. Similar to the vessels containing blood in our bodies, those microfluidic channels facilitate recirculation of a culture medium flowing inside the microfluidic device. Most often, the network consists of several channels bifurcated into two or more branches where the fluids either combine or split into different directions.

The design process of a microfluidic network is a crucial component of any microfluidic device. In his study of microfluidic blood devices Gilbert, Richards et al. pointed out that factors such as large pressure drop and complex microfluidic channel geometries limit their performance [5]. For example, studies have shown that wall shear-stress and geometry of bifurcation play crucial role in pathogenesis of artery diseases. Also, studies have shown that controlling shear stress inside microfluidic network is beneficial [6]. For instance, in some applications, maintaining low and constant shear stress through the microfluidic network is required to prevent damage of cells sensitive to shear stress, and increase their chances of binding to surfaces [7]. On the other hand, gradually increasing shear stress inside microfluidic network used in heavily-laden particulate flow is required to prevent blockage in smaller channels [7]. Moreover, high pressure drops and shear stresses inside the microfluidic network are linked directly to hemolysis and thrombosis [5]. A hemolysis condition is associated with red blood cells rupture and release of hemoglobin from within the red blood cells into the blood plasma stream while thrombosis

condition results in blood clots formation [5]. In addition, as pressure drop and flow resistance increase power needed to operate the microfluidic device increases [8]. Higher power consumption may cause increase in the device occupied volume and, thus, limit its use in several applications. In tissue engineering there is a growing need for robust microfluidic network circulation system to effectively distribute nutrients and exchange oxygen [4]. Thus, the effectiveness of the whole microfluidic device is strongly tied to the fluid flow behavior inside the microfluidic network. As a result, prediction of wall shear-stress and hydraulic resistance inside the microfluidic network, with high accuracy, is mandated [9]. Although several techniques have been reported in literature to measure wall shear-stress inside microfluidic devices [10, 11], there is lack of design rules for optimized microfluidic networks which enable precise control over wall shear-stress while maintaining uniform flow rate, minimum pressure drop, and minimum flow resistance across the microfluidic network.

One of the first few mathematical modeling work related to microfluidic network was done by Murray [12]. Murray used the principle of minimum work to derive an optimum relationship between the parent and daughter branches in cardiovascular systems. His derivation led to the well-known Murray's law which states that the cube of the diameters of the parent vessel must be equal the sum of the cubes of the daughter vessels in order to minimize the work required to maintain the flow. Here, the parent and daughter vessels refer to the original and branched microfluidic channels containing the flowing fluid. Although Murray's work is considered the most pioneer work related to design of microfluidic networks, since then, several attempts have been put forward in order to enhance the design process of microfluidic networks. For example, Oh et al. investigated the design of pressure-driven microfluidic network using analogy between fluidic system and electrical circuits [13]. In his work, pressure, flow rate, and

hydraulic resistance were analogized to voltage, current, and electrical resistance, respectively. Then, an equivalent electrical circuit was built and analyzed. Razavi et al. investigated the geometry of microfluidic network numerically [14, 15]. The model used constructal theory to optimize the performance of the network for different design parameters including cross-sectional areas, length of microfluidic channels, and the shapes of cross-section. The results from his model were in good agreement with Murray's law. Minimization of hydraulic resistance of the microfluidic network led to constant ratios between consecutive cross-sectional areas and lengths. Motivated by design of surgeries and interventions found in cardiovascular medicine Marsden et al.[16] introduced computational framework based on a derivative-free approach along with mesh adaptive direct search method to obtain a local minimum and, thus, optimized design of the microfluidic network. As an example of his computations, Marsden et al. used his computational framework to reproduce Murray's problem. Unlike Murray's original work, his computational solution was extended to consider three-dimensional pulsatile solutions of the Navier–Stokes equations and was not restricted to a Poiseuille flow assumption made by Murray. Response to pulsatile flow in microfluidic network was, also, considered by painter et al.[17], Kanaris et al.[18], and Anastasiou et al.[19]. Moreover, Barber et al.[6] investigated generalization of Murray's law to consider microfluidic network of constant-depth arbitrary shaped cross sections such as rectangular and trapezoidal cross-sectional shaped microfluidic network. In addition, using Murray's law Zografos et al.[20] studied Newtonian and power-law non-Newtonian fluid flows in constant-depth rectangular planer microfluidic network using an in-house code to perform computational fluid dynamics simulation. The model looked at shear stress and flow hydraulic resistance inside the microfluidic network. Another attempt to study the behavior of non-Newtonian blood inside a network of microfluidic channels was done by

Revellin et al.[21]. In his work, Revellin et al. derived an analytical expression of Murray's law for blood inside a circular cross-section using the power-law model assuming two different constraints in addition to the pumping power. The two constraints were volume constraint and surface constraint. His results showed that under the volume constraint, classical Murray's principle is valid and the relationship between the parent and daughter vessels is independent of the fluid properties. In contrast, under the surface constraint, different values from Murray's law may be obtained and the relationship between parent and daughters vessels depends on the fluid properties [21]. A simple model for fully developed laminar non-Newtonian fluid flow in non-circular microfluidic network was investigated by Muzychka et al. [22]. The model used power-law fluids based on Rabinowitsch–Mooney formulation and was verified for rectangular cross-sectional area within 10% accuracy. Reis et al. [23] used the constructal theory to investigate the flow inside non-symmetric network structures found in human respiratory and circulatory systems. His results showed that global flow resistances depend on the degree of asymmetry between branches in each bifurcation. Other attempts to investigate the behavior of microfluidic network include the work done by Shan *et al*. [24], Hoganson et al. [25], Gat et al.[26], Tondeur et al. [27], and Tonomura et al. [28].

The previous discussion reveals the significance of using modeling tools in understanding and improving the design of microfluidic networks widely present in microfluidic devices. The goal of the work presented in this article is to offer general guidelines for design and optimization processes of different cross-sectional shapes and geometries of microfluidic networks. In this work, wall shear-stress and hydraulic resistance inside the microfluidic network are linked directly to design parameters such as cross-sectional area and perimeter of the geometry under investigation. Distribution of wall shear-stress inside the bifurcated branches of

the microfluidic network is investigated thoroughly, and techniques for controlling shear-stress inside each microfluidic branch are provided. Similarly, minimization of hydraulic resistance through the network is investigated and connected to the microfluidic network geometry and shape. Work is carried on using a combination of multi-physics finite element COMSOL modeling and analytical techniques. The constraints used in this work are constant fluid volume flowing through the network, constant volume of network, and constant material surface area. On one hand, a constant volume flow rate constraint is drawn from the need to deliver the same amount of fluid to the designated point all the time. On the other hand, optimizing the microfluidic network requires the use of fixed surface area and minimum material upon designing the microfluidic network.

THEORY

In this section, behavior of microfluidic network is formulated. This is done by formulating the effects of geometries and dimensions on minimizing hydraulic resistances and controlling shear stresses through microfluidic networks. Figure 1 shows an example of microfluidic network used in microfluidic devices. Navier-Stokes equation is used to describe the continuous flow behavior inside the microfluidic network, given by

$$\rho \frac{\partial v}{\partial t} + \rho \boldsymbol{v} . \nabla \boldsymbol{v} = -\nabla p + \nabla . \tau \qquad (1)$$

For a fully developed, steady, laminar, and pressure-driven flow inside an arbitrary-shaped constant cross-sectional area network, shown in Figure 2, summation of forces on the channel boundaries leads to:

$$Ap_{in} - Ap_{out} - \bar{\tau} PL = 0. \qquad (2)$$

Further, pressure drop ΔP and hydraulic resistance R, are related through:

$$\Delta p = RQ, \qquad (3)$$

where Q is volume flow rate (m^3/sec), and R is hydraulic resistance for an arbitrary shaped geometry, shown in Figure 2, and given by

$$R = \frac{\mu L \beta}{A^2}. \quad (4)$$

Here, the coefficient β is geometric factor that is a linear function of compactness, i.e. C [29] given by:

$$\beta = Ca + b, \quad (5)$$

where $C = \frac{P^2}{A}$ and a & b are two constants depend on the shape of the cross-sectional area of the microfluidic channel. For example, for a rectangular cross-sectional area the geometric factor, β is given by [29]:

$$\beta = \frac{22}{7} C - \frac{65}{3}. \quad (6)$$

Using the set (2-4), the average wall shear stress $\bar{\tau}$ can be rewritten as:

$$\bar{\tau} = \beta \frac{\mu U}{P}. \qquad (7)$$

For a bifurcating network, shown in Figure 1, with an arbitrary cross-sectional shape, shown in Figure 2, a constant wall shear-stress requirement between the parent ($\bar{\tau_o}$) and the daughter ($\bar{\tau}_1$) channels, yields:

$$\beta_o \frac{\mu U_o}{P_o} = \beta_1 \frac{\mu U_1}{P_1} \qquad (8)$$

Applying the continuity equation over a control volume of the microfluidic network, gives:

$$\frac{U_1}{U_o} = 2^{-1} \frac{A_o}{A_1}. \qquad (9)$$

Substituting continuity equation (9) and the geometric factor, β (5) into (8) yields:

$$\left(\frac{P_o}{{A_o}^2}a + \frac{b}{A_o P_o}\right) = \left(\frac{P_1}{2{A_1}^2}a + \frac{b}{2A_1 P_1}\right). \qquad (10)$$

Equating the coefficients on both sides of (10) yields:

$$A_o = 2^{\frac{2}{3}} A_1 . \qquad (11\text{-a})$$

$$P_o = 2^{\frac{1}{3}} P_1 . \qquad (12\text{-a})$$

Here, the area-bifurcation ratio given in (11) is consistent with previous work reported by Razavi et al.[14]. This is, also, in agreement with Murray's original work which stated that the cube of the diameters of a circular parent vessel, D_o must be equal the sum of the cubes of the daughter vessels, D_1 in order to minimize the work required to maintain the flow. The previous derivation can be easily extended to multi-generation microfluidic network. For consecutive generation inside the microfluidic network a branching parameter, X is introduced [6, 20, 30]. The branching parameter, X is defined in terms of the ratio of the consecutive generation diameters, i.e. $X = \frac{1}{2}\left(\frac{D_i^3}{D_{i+1}^3}\right)$. Thus, for a multi-generation network, the set (11-a & 12-a) is extended to:

$$A_0 = 2^{\frac{2n}{3}} X^{\frac{2n}{3}} A_n . \qquad (11\text{-b})$$

$$P_0 = 2^{\frac{n}{3}} X^{\frac{n}{3}} P_n . \qquad (12\text{-b})$$

To investigate the effect of bifurcation ratios appearing in set (11-12), the area and perimeter power coefficients in (11-b) & (12-b) are replaced with generalized area power coefficient ($1/\alpha_1$) and generalized perimeter power coefficient ($1/\alpha_2$), respectively, yielding:

$$A_o = 2^{\frac{2n}{\alpha 1}} X^{\frac{2n}{\alpha 1}} A_n . \qquad (13)$$

$$P_o = 2^{\frac{n}{\alpha 2}} X^{\frac{n}{\alpha 2}} P_n \quad . \qquad (14)$$

Subject the microfluidic network design to constant volume, $V_{constant}$ and constant surface area, $SA_{constant}$ constraints, yields:

$$L_i A_i + 2L_{i+1} A_{i+1} = V_{constant} \qquad (15)$$

$$L_i P_i + 2L_{i+1} P_{i+1} = SA_{constant} \qquad (16)$$

For given lengths of microfluidic network and specified power coefficients, i.e. α_1 and α_2 the set (13-16) is solved to find the geometry of the parent and daughter branches. For example, consider a single generation network with rectangular cross-sectional area (Figure 1). Given, L_o, L_1, α_1 and α_2 the set (13-16) can be used to determine the widths and depths of parent and daughter branches of the microfluidic network, i.e. ω_o, D_o, ω_1, and D_1, respectively. Then, the total hydraulic resistance for bifurcating network is given by:

$$R_{total} = \frac{\mu L_0 \beta_0}{A_0^2} + \frac{\mu L_1 \beta_1}{2A_1^2} \quad , \qquad (17)$$

where $A_o = d_o \omega_o$ & $A_1 = d_1 \omega_1$ calculated using (13-16) and geometric factor, β is calculated using (6). The average wall shear-stresses, $\bar{\tau}$ in parent and daughter branches are given by (7), i.e. $\bar{\tau}_o = \beta_o \frac{\mu U_o}{P_o}$ and $\bar{\tau}_1 = \beta_1 \frac{\mu U_1}{P_1}$, respectively, and perimeters are $P_o = 2(d_o + \omega_o)$ & $P_1 = 2(d_1 + \omega_1)$.

Further, equating the coefficients in (10) and dividing the two resultant equations yields:

$$\frac{{P_0}^2}{A_0} = \frac{{P_1}^2}{A_1} = C. \quad (18)$$

Thus, an optimum design of the microfluidic network requires a fixed compactness, C of the parent and daughter branches, i.e. C_o=C_1. For a circular cross-sectional microfluidic network, the compactness of the network is always constant, i.e. C_o=C_1= 4π. However, for a rectangular cross-sectional microfluidic network the compactness within the network is dependent on the aspect ratio of the branches. Taking the square root of (18), yields:

$$\frac{P_0}{\sqrt{A_0}} = \frac{P_1}{\sqrt{A_1}}. \quad (19)$$

The ratio in (19), i.e. $\frac{P}{\sqrt{A}}$ is a non-dimensional geometrical factor [22, 31] that is related to the aspect ratio of the cross-section. For a rectangular cross-sectional microfluidic network, the factor, $\frac{P}{\sqrt{A}}$ is related to the aspect ratio by

$$\frac{P}{\sqrt{A}} = \frac{2(1+(\frac{1}{\epsilon}))}{\sqrt{1/\epsilon}}, \quad (20)$$

where ϵ is the aspect ratio of the branch, i.e. $\epsilon = \frac{\omega}{d}$. The set (18 & 20) indicates that for an optimal network design, aspect ratio should be fixed throughout the network. Thus, to find compactness, C and aspect ratio, ϵ that correspond to minimum hydraulic resistance, the sets (11-b,15,18) and (11-b,15,19,20) are solved, respectively. The compactness, C obtained is then substituted in (6, 17) to calculate the hydraulic resistance.

Similar argument can be carried for different cross-sectional shapes found in microfabrication. For example, akin to the procedure described above one can obtain an optimal design of a triangular cross-sectional area microfluidic network. For instance, the compactness of an isosceles triangular cross-sectional area microfluidic network is given by:

$$C = \frac{((2*l)+B)^2}{\frac{1}{2}B^2\sqrt{\frac{l^2}{B^2}-\frac{1}{4}}}, \qquad (21)$$

where l is one of the two equal sides (leg length) and B is the base of the triangle. To find the optimum C of the network, equation (21) is solved for parent and daughter branches along with set (11-b, 15). Hydraulic resistance is then obtained using (17) , where the geometric factor β is given by [29]:

$$\beta = \frac{25}{17}C + \frac{40\sqrt{3}}{17}. \quad (22)$$

RESULTS AND DISCUSSION

To investigate the performance of various microfluidic networks the multi-physics modeling COMSOL software is used to run the simulation. Since Navier-Stokes equation is valid for continuous fluid, first the continuum assumption is verified for the microfluidic network by calculating Knudsen number, k_n. For a 1μm characteristic length and using liquid water as a working fluid the estimated Knudsen number is k_n =3x10^{-4} which is smaller than the critical value for continuum assumption, i.e. 1x10^{-3}[32]. For the geometry considered in this article, the smallest characteristic length is larger than 1μm and, thus, the continuous flow assumption is valid.

First, single-generation microfluidic network is investigated. Table I lists geometric parameters and flow conditions used in simulation. Figure 3-5 shows model and analytical results of flow inside rectangular cross-sectional area, T-shaped, single generation microfluidic network. Both hydraulic resistance R, and wall shear-stress ratio $\frac{\bar{\tau}_{inlet}}{\bar{\tau}_{outlet}}$ across the microfluidic network versus area power coefficient, α_1, are shown. In Figure 3-5 the perimeter power

coefficients α_2 are held constant, i.e. α_2=2, 3, and 4.5, respectively. For both wall shear-stress and hydraulic resistance the figures reveal good agreement between model simulation and analytical results obtained using (7) and (17), respectively. Discrepancies between model simulation and analytical results are, possibly, attributed to irregularities in flow field near inlet of bifurcations accounted for in simulation. Nonetheless, for small Reynold numbers pressure losses around junctions and corners can be neglected for calculating hydraulic resistances. Nonetheless, maximum error in modeled hydraulic resistances is 1.00%, 1.35%, and 1.6%, respectively. While the error is very small, the Y-axis scale is magnified, in the figures, to show the points of minimum hydraulic resistances. Similar behavior is observed for pressure drop and power loss through the microfluidic network.

The figures, also, reveal the behavior of hydraulic resistance and wall shear-stress. On one hand, for a fixed perimeter power coefficient, α_2 as the area power coefficient, α_1 increased the flow resistance degrades to a minimum point and then increases again. On the other hand, the figures also suggest that increasing perimeter power coefficient, α_2 while fixing the area power coefficient, α_1 will reduce the minimum hydraulic resistance, R_{min} further. That is, for the three perimeter power coefficients cases considered here, i.e. α_2=2, 3, and 4.5 the minimum hydraulic resistances are, R_{min}= $2.9136\text{x}10^{11}\frac{kg}{m^4.s}$ (at α_1=2.6,$\epsilon_0 = 2.5852, \epsilon_1 = 1.6197$), $2.865\text{x}10^{11}\frac{kg}{m^4.s}$ (at α_1=3.0, $\epsilon_0 = 2.0012, \epsilon_1 = 2.0012$), and $2.820\text{x}10^{11}\frac{kg}{m^4.s}$ (at α_1=3.3,$\epsilon_0 = 1.5362, \epsilon_1 = 2.2364$), respectively. Thus, larger perimeter power coefficients, α_2 caused hydraulic resistance curves shown in Figure 3-5 to shift further down. However, the wall shear-stress ratio $\frac{\bar{\tau}_{inlet}}{\bar{\tau}_{outlet}}$ increased continuously as the area power coefficient, α_1 increased. Thus, one can notice that to, simultaneously, achieve a minimum "local" hydraulic resistance, i.e. R=$R_{\min}$

and constant wall shear-stress through the microfluidic network, i.e. $\frac{\bar{\tau}_{inlet}}{\bar{\tau}_{outlet}}$=1, both area power coefficient and perimeter power coefficient must equal 3, i.e. α_1=α_2=3. It is, also, noteworthy to mention that for this optimal case, i.e.α_1=α_2=3 the aspect ratios of parent and daughter branches are constant, i.e. $\epsilon_0 = \epsilon_1 = 2.0012$.

Figure 6 reveals the effect of width, ω to depth, d aspect ratio, i.e. $\epsilon = \frac{\omega}{d}$ on the performance of a rectangular cross-section microfluidic network. Here, both area power coefficient and perimeter power coefficient are set optimum, i.e. α_1=α_2=3. Figure 6 reveals that each aspect ratio, $\epsilon = \frac{\omega}{d}$ will have a minimum "local" hydraulic resistance when α_1=α_2=3. Nonetheless, a "global" minimum hydraulic resistance occurs, only, when the aspect ratio is set to unity, i.e. $\epsilon = 1$ (where the corsponding optimum compactness C is 16). This is, also, evident in theoretical results shown in Figure 6 and obtained by solving the set (11-b, 15, 19, 20). Good agreement between modeled and theoretical results is apparent. Thus, a square cross-sectional shaped microfluidic network is the optimal design between all rectangular cross-sectional microfluidic networks. Similarly, by solving the set (11-b, 15, 21) for a isosceles triangular cross-sectional area microfluidic network results reveal that "global" minimum hydraulic resistance occurs at compactness, C = 21 which is close to the compactness of an equilateral (regular isosceles) triangular cross-sectional area, i.e. C=20.7846. Like the square cross-sectional area, all sides and angles are equal in the equilateral triangular cross-sectional area. This suggests that the optimal design of any shape is the regular case. Furthermore, calculating the hydraulic resistances for isosceles triangular, circular, and rectangular cross-sectional area microfluidic networks (for same flow conditions and optimal configurations) yields, R= 6.4902 × $10^{11}\frac{kg}{m^4.s}$, 2.06×$10^{11}\frac{kg}{m^4.s}$, and 2.35 × $10^{11}\frac{kg}{m^4.s}$, respectively. Thus, for same

conditions, a microfluidic network with circular cross-sectional area performs better compared to rectangular and isosceles triangular cross-sectional area microfluidic networks.

Figure 7-9 shows multi-generation microfluidic network behavior for branching parameter, X=0.7, 1.0, and 1.5, respectively. Table II lists all parameters used in multi-generation microfluidic network simulation. Here, both optimum area power coefficient and perimeter power coefficient are used, i.e. $\alpha_1=\alpha_2=3$. Figure 7-9 demonstrates a successful design of microfluidic network with precise control over wall shear-stress from one generation to another. Figure 7 shows gradually decreasing wall shear-stress along the microfluidic network. Figure 7-a shows modeled and analytical wall shear-stress in n-generation, average $\overline{\tau}_n$ normalized against the average wall shear-stress at the inlet of the microfluidic network, $\overline{\tau}_{o,inlet}$. The figure reveals that average wall shear-stress is steadily lowered in the microfluidic network from wall shear-stress ratio, $\frac{\bar{\tau}_n}{\bar{\tau}_{o,inlet}} = 1$ for n=0 to wall shear-stress ratio, $\frac{\bar{\tau}_n}{\bar{\tau}_{o,inlet}} = 0.34$ for n=3. This is, also, evident in Figure 7-b which shows COMSOL simulated wall shear-stress in the microfluidic network. Similarly, Figure 8 presents a multi-generation microfluidic network design with branching parameter, X=1 suitable for application where constant wall shear-stress is required through the network. Here, average wall shear-stress is maintained constant through the microfluidic network, i.e. $\frac{\bar{\tau}_n}{\bar{\tau}_{o,inlet}} = 1$. Lastly, for applications where wall shear-stress needs to steadily be increased Figure 9 shows the case. Here, average wall shear-stress is gradually increased in the microfluidic network from wall shear-stress ratio, $\frac{\bar{\tau}_n}{\bar{\tau}_{o,inlet}} = 1$ for n=0 to wall shear-stress ratio, $\frac{\bar{\tau}_n}{\bar{\tau}_{o,inlet}} = 3.37$ for n=3. Results from COMSOL simulation are in good agreement with theoretical results obtained using (7). Similar behavior was reported in the literature [6].

Figure 10 shows normalized wall-shear stress distribution in each generation, n of the multi-generation microfluidic network for branching parameter, X=1 obtained using our work (Figure 10-a) and theory reported in [6, 30] (Figure 10-b). In Figure 10-a, wall-shear stress distribution in each generation of the rectangular cross-section multi-depth network reported in this work is normalized against mean wall shear stress at the inlet channel, n=0. Figure 10-b shows the normalized wall-shear stress distribution for a rectangular constant-depth multi-generation network reported in [6, 30] . The superiority of the design reported in this work is evident in Figure 10. That is, Figure 10-a shows that profiles of wall-shear stresses are successfully maintained identical throughout all the generations of the multi-depth microfluidic network. This is, presumably, because compactness, and thus, aspect ratio, is maintained the same in our multi-depth microfluidic network design. This fixed compactness and aspect ratio is achieved by allowing the depth of each generation in the microfluidic network to change along with the width. Nonetheless, the profiles of wall-shear stresses shifted to a lower value from one generation to another in Figure 10-b where rectangular constant-depth generations is used. Thus, compactness and aspect ratio varied from one generation to another in Figure 10-b which led to the observed wall-shear stress behavior.

CONCLUSION

Continuous developments in *lap-on-chip* fabrication has resulted in complex microfluidic networks. Such microfluidic networks are required to operate in optimum fashion where hydraulic resistance and pressure drop are minimized while wall shear-stress is precisely mapped through the network. For instance, in some applications, maintaining constant shear stress through the microfluidic network is required to prevent damage of cells sensitive to shear stress. In other applications such as heavily-laden particulate flow, gradually increasing shear stress inside microfluidic network is required to prevent blockage in smaller channels. A combination of theoretical and modeling techniques is used to construct microfluidic networks that achieve the condition of minimum hydraulic resistance and pressure drop while, simultaneously, maintaining high control over wall shear-stress throughout the network. Constraints imposed

include constant network volume, constant surface area and constant flow rate. Results obtained from model are in good agreement with theoretical outcomes. The results show that a global minimum hydraulic resistance is achieved when certain geometric conditions are satisfied. These geometric conditions are related to choosing both perimeter and area, and thus compactness and aspect ratio, of parent and daughter branches. The results show that for rectangular cross-sectional area microfluidic network, the global minimum hydraulic resistance is obtained when aspect ratio is set to unity, i.e. square-cross sectional area. Similarly, the global minimum hydraulic resistance for isosceles triangular cross-sectional area microfluidic network is achieved when all triangle sides are equal in length (Equilateral Triangle). The work, also, demonstrates successful design guidelines for the purpose of controlling wall shear-stress through the bifurcations of the microfluidic network. Increasing, decreasing, and constant wall shear-stress through a rectangular T-shaped microfluidic network are, also, presented.

REFERENCES

1. Huh, D., et al., *Reconstituting organ-level lung functions on a chip.* Science, 2010. **328**(5986): p. 1662-1668.
2. Huh, D., et al., *Microengineered physiological biomimicry: organs-on-chips.* Lab on a chip, 2012. **12**(12): p. 2156-2164.
3. Potkay, J.A., et al., *Bio-inspired, efficient, artificial lung employing air as the ventilating gas.* Lab on a Chip, 2011. **11**(17): p. 2901-2909.
4. Barber, R.W. and D.R. Emerson, *Biomimetic design of artificial micro-vasculatures for tissue engineering.* Altern Lab Anim, 2010. **38**(Suppl 1): p. 67-79.
5. Gilbert, R.J., et al., *Computational and functional evaluation of a microfluidic blood flow device.* Asaio Journal, 2007. **53**(4): p. 447-455.
6. Barber, R.W. and D.R. Emerson, *Optimal design of microfluidic networks using biologically inspired principles.* Microfluidics and Nanofluidics, 2008. **4**(3): p. 179-191.
7. Auniņš, J.G., et al., *Fluid mechanics, cell distribution, and environment in cell cube bioreactors.* Biotechnology progress, 2003. **19**(1): p. 2-8.
8. Wang, L., Y. Fan, and L. Luo, *Lattice Boltzmann method for shape optimization of fluid distributor.* Computers & Fluids, 2014. **94**: p. 49-57.
9. Berthier, J., et al. *COMSOL assistance for the determination of pressure drops in complex microfluidic channels*. in *Comsol Conference*. 2010.
10. Wu, J., D. Day, and M. Gu, *Shear stress mapping in microfluidic devices by optical tweezers.* Optics express, 2010. **18**(8): p. 7611-7616.
11. Cioffi, M., et al., *A computational and experimental study inside microfluidic systems: the role of shear stress and flow recirculation in cell docking.* Biomedical microdevices, 2010. **12**(4): p. 619-626.
12. Murray, C.D., *The physiological principle of minimum work: I. The vascular system and the cost of blood volume.* Proceedings of the National Academy of Sciences of the United States of America, 1926. **12**(3): p. 207.
13. Oh, K.W., et al., *Design of pressure-driven microfluidic networks using electric circuit analogy.* Lab on a Chip, 2012. **12**(3): p. 515-545.
14. Razavi, M.S., E. Shirani, and M. Salimpour, *Development of a general method for obtaining the geometry of microfluidic networks.* AIP Advances, 2014. **4**(1): p. 017109.

15. Sayed Razavi, M. and E. Shirani, *Development of a general method for designing microvascular networks using distribution of wall shear stress.* Journal of biomechanics, 2013. **46**(13): p. 2303-2309.
16. Marsden, A.L., J.A. Feinstein, and C.A. Taylor, *A computational framework for derivative-free optimization of cardiovascular geometries.* Computer methods in applied mechanics and engineering, 2008. **197**(21): p. 1890-1905.
17. Painter, P.R., P. Edén, and H.-U. Bengtsson, *Pulsatile blood flow, shear force, energy dissipation and Murray's Law.* Theoretical Biology and Medical Modelling, 2006. **3**(1): p. 31.
18. Kanaris, A., A. Anastasiou, and S. Paras, *Numerical study of pulsatile blood flow in micro channels.*
19. Anastasiou, A., A. Spyrogianni, and S. Paras. *Experimental study of pulsatile blood flow in micro channels*. in *CHISA 2010, 19th International Congress of Chemical and Process Engineering*. 2010.
20. Zografos, K., et al., *Constant depth microfluidic networks based on a generalised Murray's law for Newtonian and power-law fluids.* 2014.
21. Revellin, R., et al., *Extension of Murray's law using a non-Newtonian model of blood flow.* Theoretical Biology and Medical Modelling, 2009. **6**(1): p. 7-9.
22. Muzychka, Y. and J. Edge, *Laminar non-Newtonian fluid flow in noncircular ducts and microchannels.* Journal of Fluids Engineering, 2008. **130**(11): p. 111201.
23. Reis, A.H., *Laws of non-symmetric optimal flow structures, from the macro to the micro scale.* 2012.
24. Shan, X., M. Wang, and Z. Guo, *Geometry optimization of self-similar transport network.* Mathematical Problems in Engineering, 2011. **2011**.
25. Hoganson, D.M., et al., *Principles of biomimetic vascular network design applied to a tissue-engineered liver scaffold.* Tissue Engineering Part A, 2010. **16**(5): p. 1469-1477.
26. Gat, A.D., I. Frankel, and D. Weihs, *Compressible flows through micro-channels with sharp edged turns and bifurcations.* Microfluidics and Nanofluidics, 2010. **8**(5): p. 619-629.
27. Tondeur, D., Y. Fan, and L. Luo, *Constructal optimization of arborescent structures with flow singularities.* Chemical Engineering Science, 2009. **64**(18): p. 3968-3982.
28. Tonomura, O., et al. *Optimal Shape Design of Pressure-Driven Microchannels using Adjoint Variable Method*. in *ASME 2007 5th International Conference on Nanochannels, Microchannels, and Minichannels*. 2007. American Society of Mechanical Engineers.
29. Mortensen, N.A., F. Okkels, and H. Bruus, *Reexamination of Hagen-Poiseuille flow: Shape dependence of the hydraulic resistance in microchannels.* Physical Review E, 2005. **71**(5): p. 057301.
30. Emerson, D.R., et al., *Biomimetic design of microfluidic manifolds based on a generalised Murray's law.* Lab on a Chip, 2006. **6**(3): p. 447-454.
31. Bahrami, M., M. Yovanovich, and J. Culham, *Pressure drop of fully-developed, laminar flow in microchannels of arbitrary cross-section.* Journal of Fluids Engineering, 2006. **128**(5): p. 1036-1044.
32. Gadad, P., et al., *Numerical Study of Flow inside the Micro Fluidic Cell Sense Cartridge.* APCBEE Procedia, 2014. **9**: p. 59-64.

NOMENCLATURE

Symbol	Description	Unit
A	Area	m^2
a	Geometric Constant	-
b	Geometric Constant	-
B	Base Length in Isosceles Triangle	m
C	Compactness Ratio	-
d	depth	m
L	Length	m
l	Leg Length in Isosceles Triangle	m
n	Micro-channel generation	-
P	Perimeter	m
p	Pressure	Pa
Q	Volumetric Flow Rate	m^3/s
R	Hydraulic Resistance	$Kg/(m^4.s)$
U	Average Velocity	m/s
V	Volume	m^3
X	Branching Parameter	-
SA	Surface Area	m^2
	Greek Symbols	
μ	Dynamic Viscosity	Pa.s
β	Geometric factor	-
$\bar{\tau}$	Average Wall Shear Stress	Pa
α_1	Generalized Area Power Coefficient	-
α_2	Generalized Perimeter Power Coefficient	-
ω	width	m
ϵ	Aspect ratio	-
	Subscript	
in	Inlet	
out	Outlet	
0	Parent channel	
1	Daughter channel	

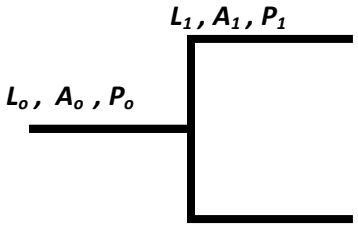

Figure 1: Example of microfluidic network used in microfluidic devices.

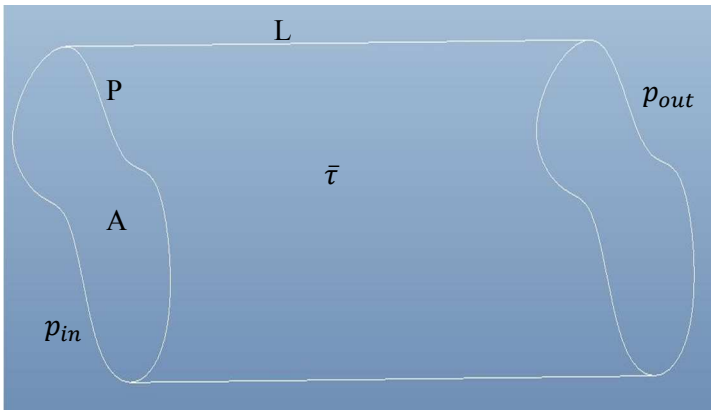

Figure 2: Arbitrary shaped constant cross-sectional area microfluidic channel.

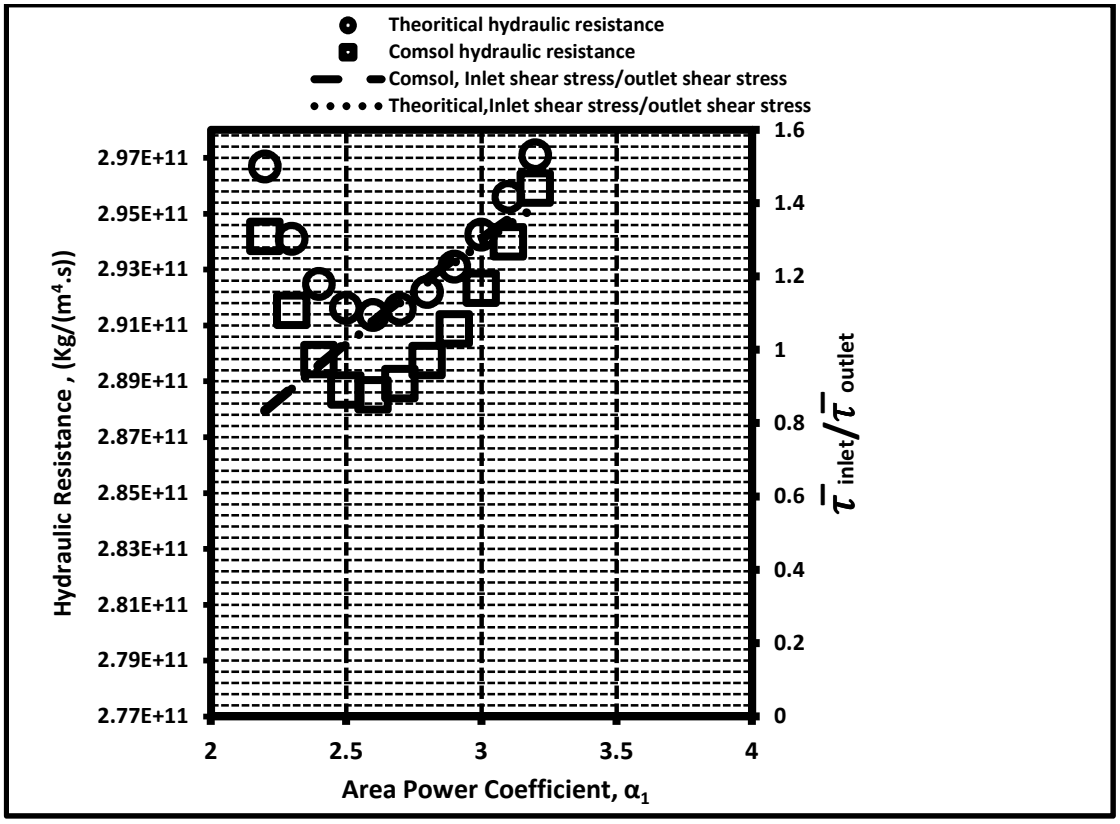

Figure 3: Model and analytical results of wall shear-stress and hydraulic resistance of a single-generation rectangular cross-sectional area, T-shaped, microfluidic network. Perimeter power coefficient, α_2=2

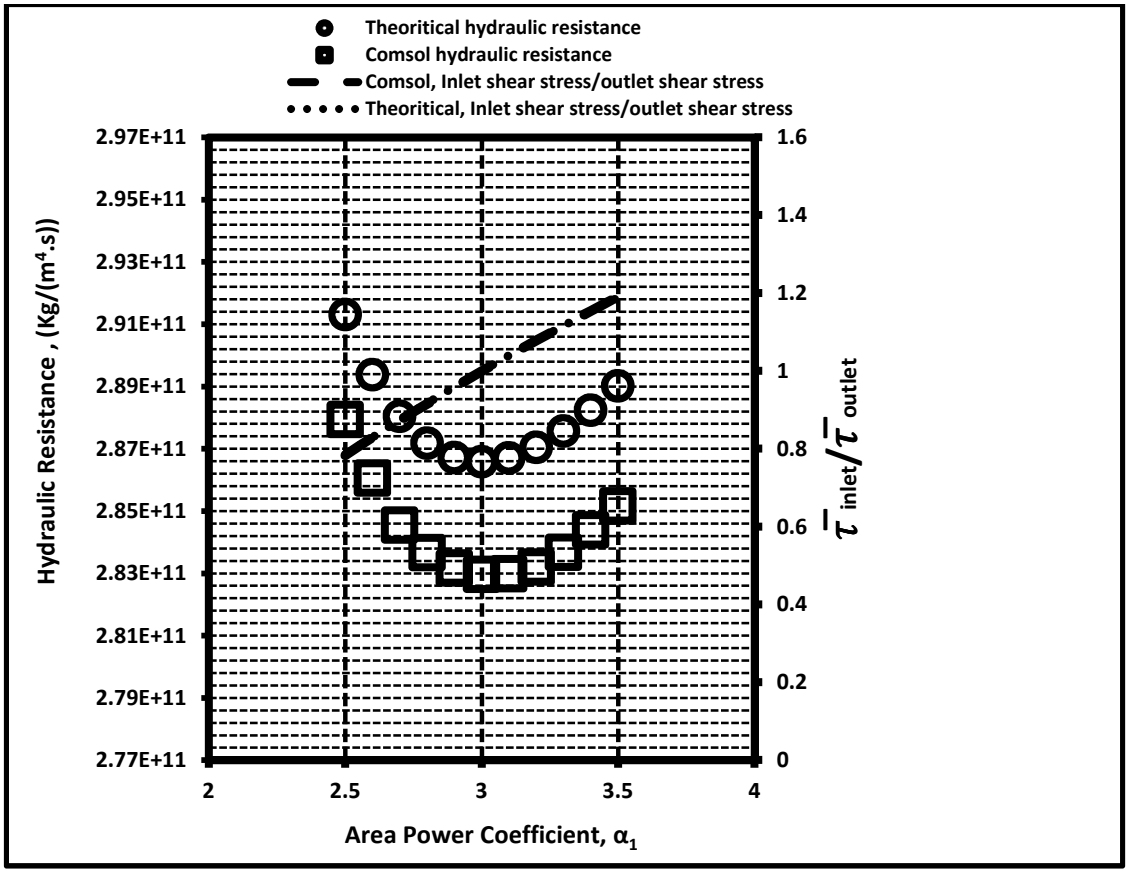

Figure 4: Model and analytical results of wall shear-stress and hydraulic resistance of a single-generation rectangular cross-sectional area, T-shaped, microfluidic network. Perimeter power coefficient, α_2=3

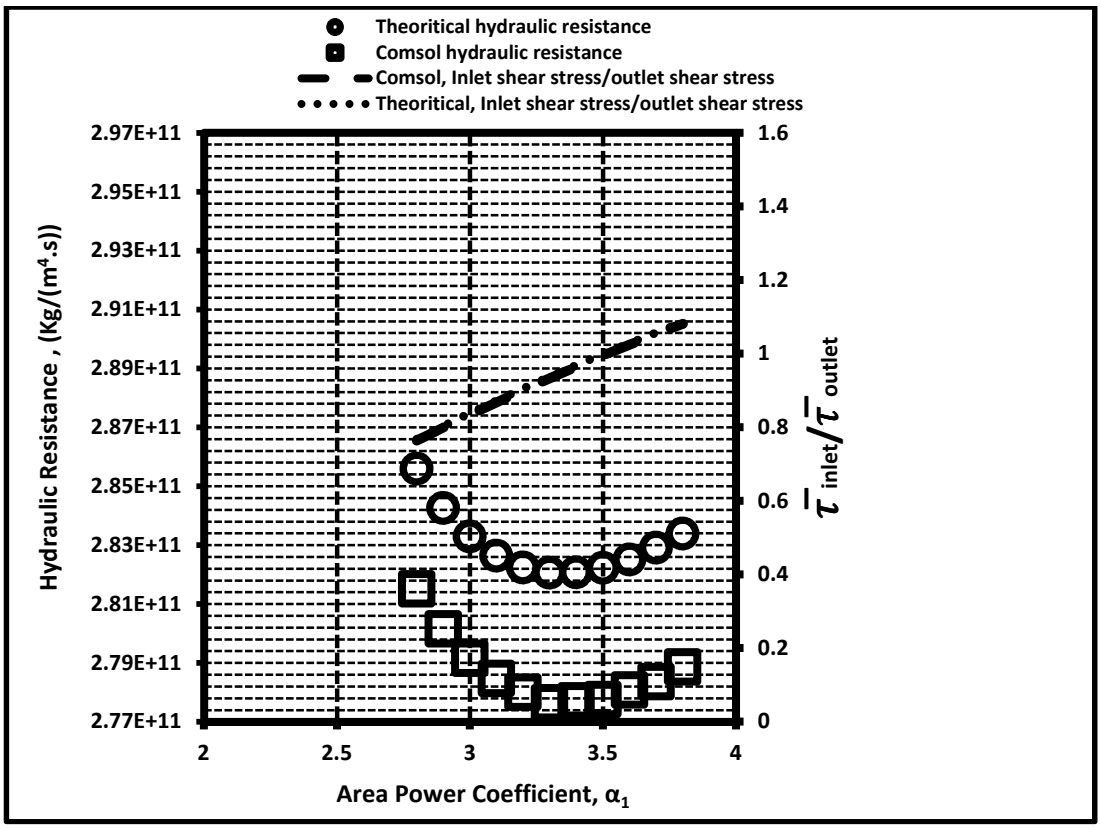

Figure 5: Model and analytical results of wall shear-stress and hydraulic resistance of a single-generation rectangular cross-sectional area, T-shaped, microfluidic network. Perimeter power coefficient, α_2=4.5

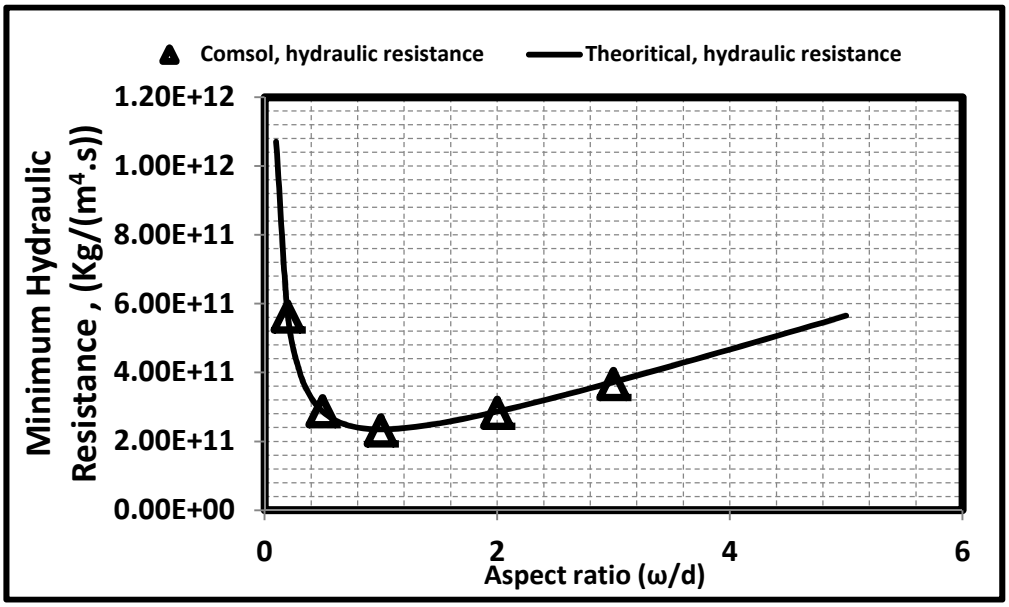

Figure 6: Effect of aspect ratio, ϵ on the performance of rectangular cross-sectional area microfluidic network.

a

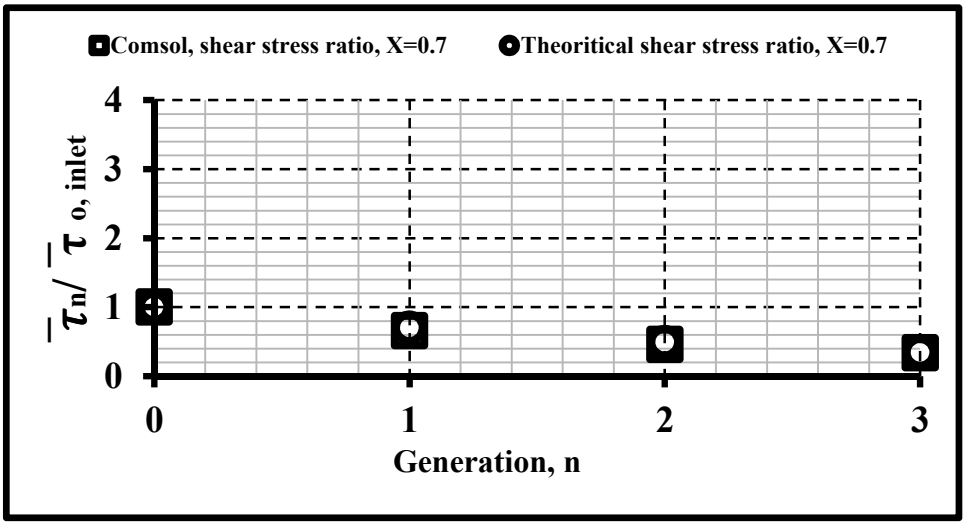

b

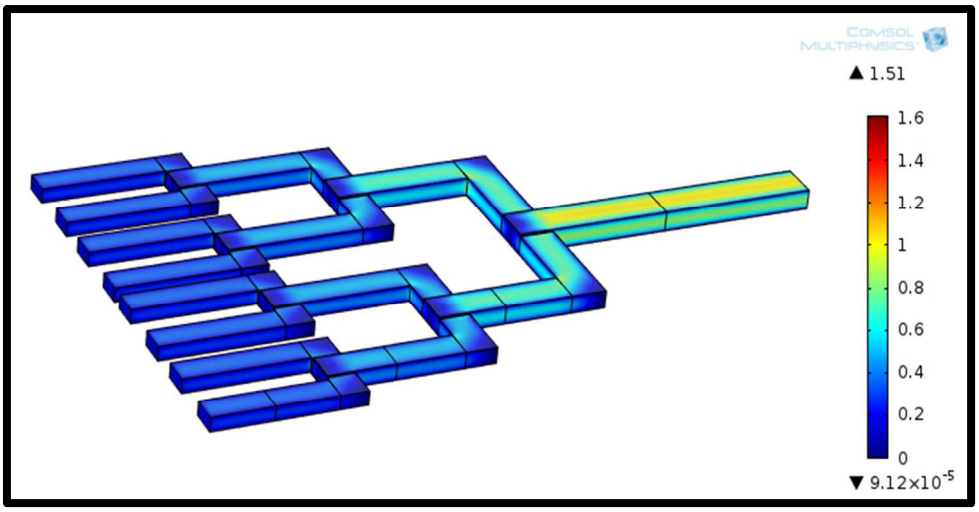

Figure 7: Mutli-generation microfluidic network, *X*=0.7. Control of total wall shear-stress in n-generation with respect to inlet wall shear stress (a). COMSOL generated wall shear-stress distribution in n-generation (b).

a

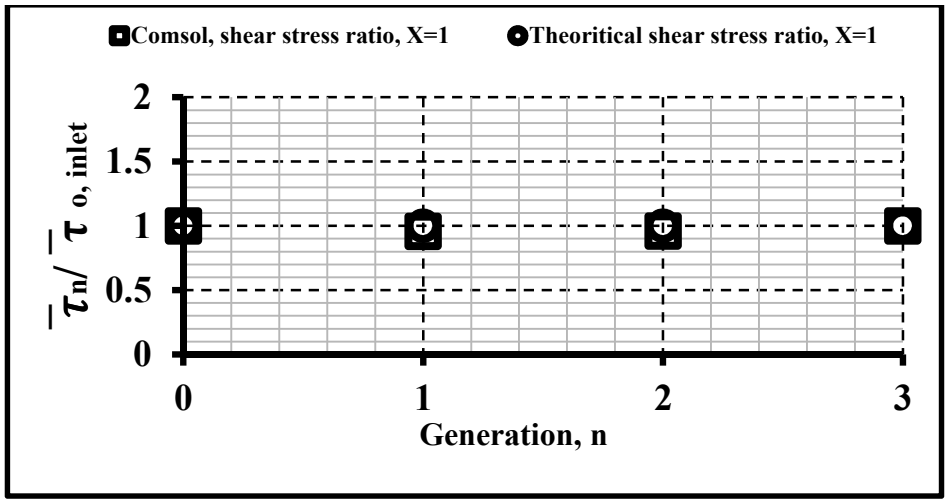

b

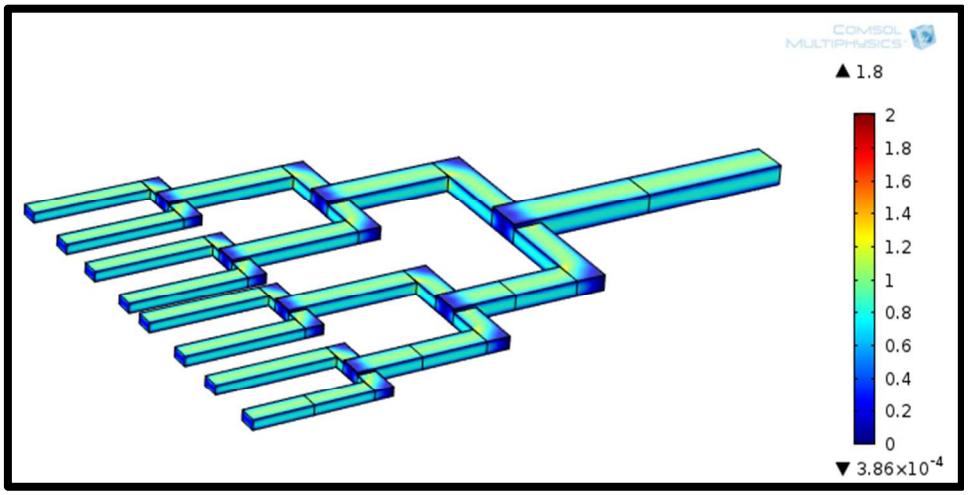

Figure 8: Mutli-generation microfluidic network, *X*=1.0. Control of total wall shear-stress in n-generation with respect to inlet wall shear stress (a). COMSOL generated wall shear-stress distribution in n-generation (b).

a

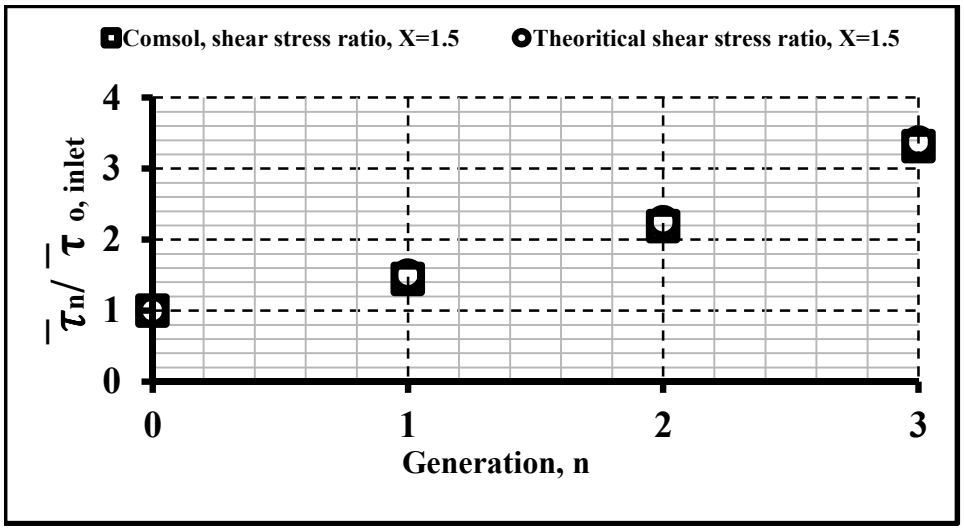

b

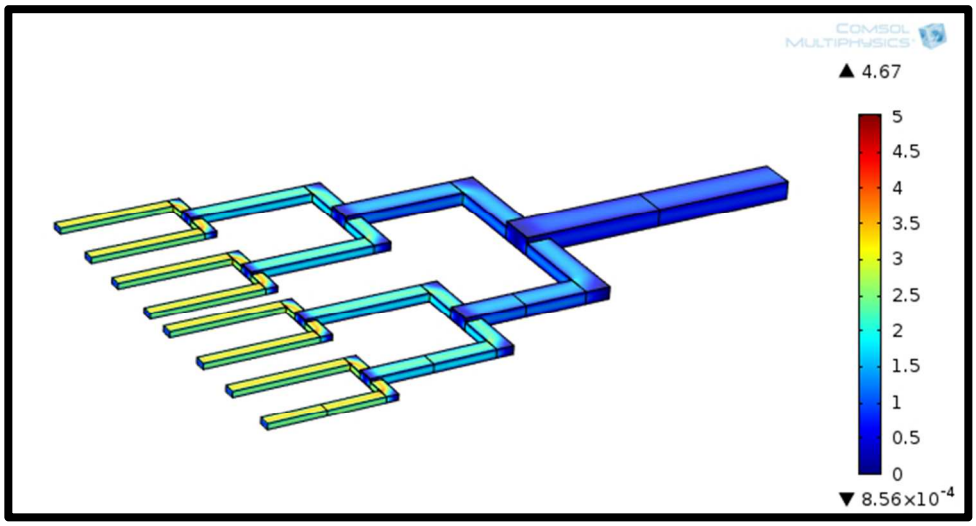

Figure 9: Mutli-generation microfluidic network, *X*=1.5. Control of total wall shear-stress in n-generation with respect to inlet wall shear stress (a). COMSOL generated wall shear-stress distribution in n-generation (b).

a

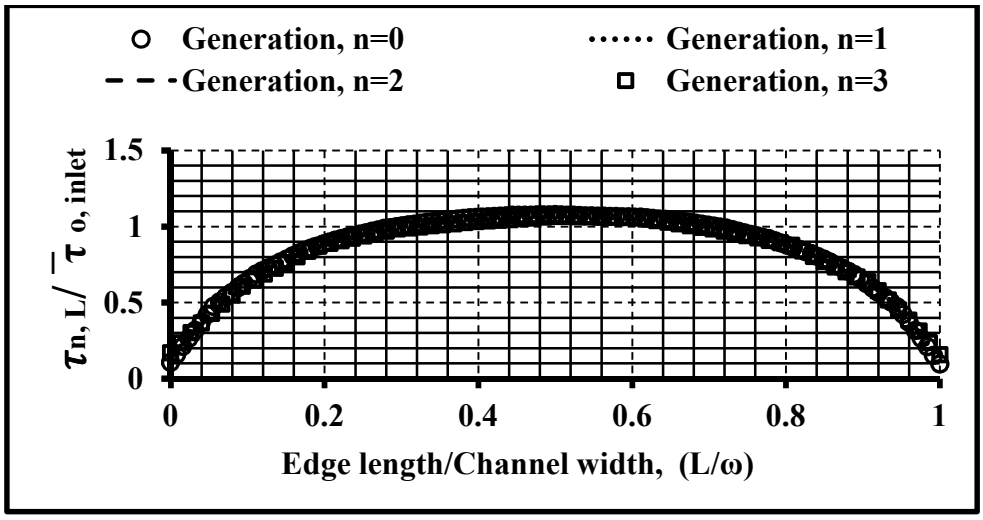

b

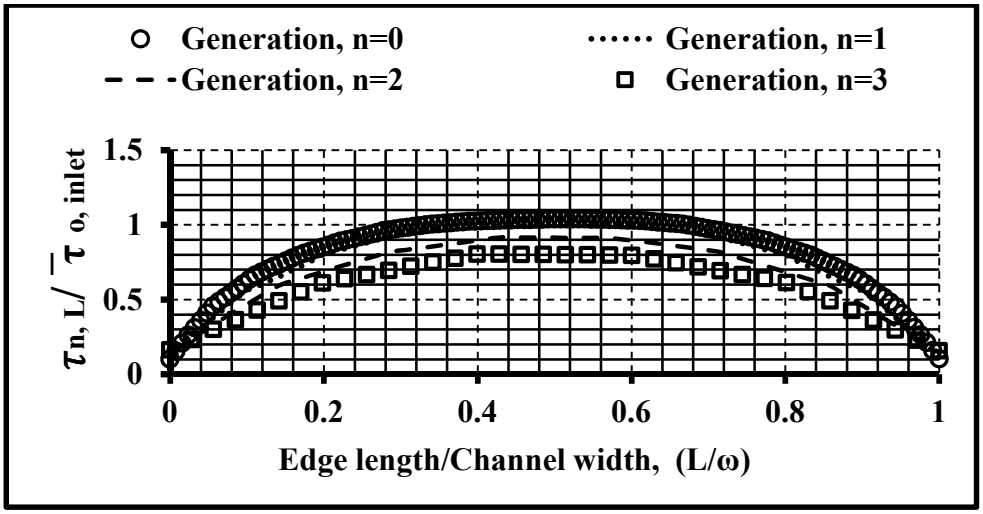

Figure 10: Normalized wall shear stress distributions calculated using Comsol along the middle upper edge in each generation, *n* at *X*=1. Wall shear stress is normalized against the average shear stress in the inlet channel, *n*=0. The edge length is normalized against the channel width in each generation. a) This work b) Using theory reported in [6, 30].

Table I: Single-generation microfluidic network simulation parameters.

Software and Solver	
Software	Comsol Multiphysics 4.4
Geometry Software	Solid Works 2014
Supplementary software	Matlab R2013a
Physics Type (In Comsol)	Laminar Flow
Simulation Type (Transient or steady)	Steady (Stationary Solver)
Main solver (Coupled or segregated)	Fully Coupled
Linear solver (Direct or iterative)	Iterative
Geometry	
Network inlet length (n=0)	4 mm
Single-generation length (n=1)	4 mm
Network total volume ($V_{constant}$)	3e-10 m^3
Network total surface area ($SA_{constant}$)	8e-06 m^2
Mesh	
Number of elements	(600,000-1000,000)
Elements type	Tetrahedral and Prism element type
Flow properties	
Material	Water
Viscosity	0.001 Pa.s
Density	1000 kg/m^3
Reynolds number	2.4142-2.8383
Boundary Conditions	
Inlet condition	Constant flow rate (5e-10 m^3/s)
Outlet condition	Constant pressure (0 Pa,gage)
Walls	No slip condition

Table II: Multi-generation microfluidic network simulation parameters.

Software and Solver	
Software	Comsol Multiphysics 4.4
Geometry Software	Solid Works 2014
Supplementary	Matlab R2013a
Physics Type (In Comsol)	Laminar Flow
Simulation Type (Transient or steady)	Steady (Stationary Solver)
Main solver (Coupled or segregated)	Fully Coupled
Linear solver (Direct or iterative)	Iterative
Geometry	
Network inlet width, ω_o	0.25 mm
Network inlet depth, D_o	0.125 mm
Aspect ratio ϵ (Constant throughout the network)	2
Network inlet length, *Lo*	2 mm
Consecutive length, L_{i+1}	$L_{i+1} = \frac{L_i}{2^{1/3}}$ [14]
Mesh	
Number of elements	(1200,000 -2200,000)
Elements type	Tetrahedral and Prism element type
Simulation Parameters	
Material	Water
Viscosity	0.001 Pa.s
Density	1000 kg/m^3
Reynolds number	2.67
Boundary Conditions	
Inlet condition	Constant flow rate (5e-10 m^3/s)
Outlet condition	Constant pressure (0 Pa, gage)
Walls	No slip condition